J. Fluid Mech. (1991), *vol.* 222, *pp.* 231–250
Printed in Great Britain

A computational study of Rayleigh–Bénard convection. Part 1. Rayleigh-number scaling

By ANIL E. DEANE† AND LAWRENCE SIROVICH
Center for Fluid Mechanics *and* The Division of Applied Mathematics, Brown University, Providence, RI 02912, USA

(Received 14 February 1989 and in revised form 13 February 1990)

A parametric study is made of chaotic Rayleigh–Bénard convection over moderate Rayleigh numbers. As a basis for comparison over the Rayleigh number (*Ra*) range we consider mean quantities, r.m.s. fluctuations, Reynolds number, probability distributions and power spectra. As a further means of investigating the flow we use the Karhunen–Loéve procedure (empirical eigenfunctions, proper orthogonal decomposition). Thus, we also examine the variation in eigenfunctions with *Ra*. This in turn provides an analytical basis for describing the manner in which the chaos is *enriched* both temporarily and spatially as *Ra* increases. As *Ra* decreases, the significant mode count decreases but, in addition, the eigenfunctions tend more nearly to the eigenfunctions of linearized theory. As part of this parametric study a variety of scaling properties are investigated. For example it is found that the empirical eigenfunctions themselves show a simple scaling in *Ra*.

1. Introduction

Rayleigh–Bénard convection is of fundamental importance to fluid mechanics not only because of applications to natural phenomena but also because it is a basic model system which incorporates dissipation and nonlinearity and which exhibits turbulence. In this paper and that which follows (Sirovich & Deane 1990, hereinafter referred to as II) we explore a range of flows in which the Rayleigh number (*Ra*) varies. This section serves as an introduction to both parts.

Rayleigh–Bénard convection has shown fresh vitality partly as a result of new ideas associated with what might be called the *chaotic dynamics* of dissipative systems. In brief, this collection of ideas which suggest routes to chaos (Ruelle & Takens 1971) other than the classical picture (Landau 1944), introduces the idea that there are certain universal features (Feigenbaum 1978) and demonstrates that small dynamical systems, corresponding to relatively smooth spatial structures, can lead to chaotic behaviour (Lorenz 1963). An additional concept within this framework, and one which we shall dwell on, is the idea that dissipative systems possess relatively low-dimensional attractors. Thus, although the representational phase space for the Boussinesq equations of turbulent thermal convection is infinite-dimensional, the trajectory of the system is drawn into a finite-dimensional attracting set as a result of dissipation. In the case of two-dimensional convection this has been proven by Constantin *et al.* (1985) and Foiaş, Manley & Temam (1987). For relatively low values of *Ra*, which is the active control parameter for Rayleigh–Bénard convection, this attracting set can be a point (zero dimension), a

† Present address: Applied and Computational Mathematics, Princeton University, Princeton, NJ 08544, USA

ring (one dimension), or a two-torus (two dimensions) depending on whether the motion is steady, single-frequency, or two-frequency. A comprehensive review is to be found in the article by Busse (1985).

At higher values of the control parameter for this and similar dissipative systems, the belief is the trajectory is drawn into a non-simple attracting set of relatively low dimension. Once on this attracting set, nearby trajectories separate exponentially fast – which makes the attractor *strange*. For Rayleigh–Bénard convection there is experimental confirmation for this view (Malraison *et al.* 1983). It is further thought that the dimension of the attractor increases gradually with increasing Ra. More generally this is held to be the case for other closed systems, e.g. Taylor–Couette flow (Fenstermacher, Swinney & Gollub 1979). By contrast open systems such as boundary layers, Poiseuille flow and so forth show a dramatic increase in attractor dimension once the system is beyond the critical value. Keefe & Moin (1987) have already presented evidence for this in the case of channel flow.

The present investigation originates in a recent, thorough numerical study of low-aspect-ratio Rayleigh–Bénard convection performed at seventy times the critical Rayleigh number, $70Ra_c$ (Sirovich, Maxey & Tarman 1989*b*; Tarman 1989). It was found that at that value of Ra, the turbulent motion was sluggish and probably better termed chaos. The basic motion of the fluid was found to be counter-rotating rolls raising heated fluid and lowering cooled fluid. At seemingly random times the axes of the cells themselves rotated by $\pm\frac{1}{2}\pi$ in the horizontal. Although many modes participate in the total flow, roughly 40% of the energy of the motion was accounted for by the simple cellular patterns just described. Moreover, although the numerical simulation required a phase space of roughly 10^5 dimensions, a reasonably accurate picture describing more than 90% of the energy was possible in terms of a subspace of roughly 320 dimensions.

One of the goals of the present investigation (dealt with in II) is to accurately estimate the dimension of the attractor of this flow. In addition, we shall also describe the change in the nature of the flow and in particular the attractor dimension as the Rayleigh number is varied from its near critical value to the maximum considered by us, $70Ra_c$. The basis for our dimension estimates is the Kaplan–Yorke (1979) formula, which in turn depends on the calculation of the Lyapunov spectrum. As is well known (Shimada & Nagashima 1979; Benettin *et al.* 1980; Wolf *et al.* 1985) such calculations are computationally intensive. (Each computation of a Lyapunov experiment requires the equivalent of an additional full simulation.) For this reason we adopt (and justify the use of) a coarse-grained version of the direct simulation. In this connection mention should be made of the coarse-grain calculations of Gilbert & Kleiser (1987) for the channel problem. Some of our arguments may shed light on the almost unreasonable success of their computations. In addition we also introduce some approximate methods for the determination of the Lyapunov dimension without fully determining the Lyapunov spectrum.

In the already mentioned earlier treatment, the Karhunen–Loéve (K-L) procedure (Ash & Gardner 1975; Lumley 1970) played an essential role in the analysis of the turbulent flow. This method, which was introduced into turbulence theory by Lumley in a pioneering paper (Lumley 1967), has been important in a variety of problems (Moin 1984; Moin & Moser 1989; Sirovich & Rodriguez 1987; Aubry *et al.* 1988; Glauser, Lieb & George 1987). For a history of this method see Preisendorfer (1988). Within the framework of second-order statistics it can be shown that the K-L method gives an optimally compact description of the turbulent flow. It is therefore of interest to see how the intrinsic dimension of the K-L description

compares with the Lyapunov dimension (which in a sense gives the ideal value). This we do over a range of Rayleigh numbers. In this light we also compare the K-L eigenfunctions as Ra is varied and observe mode crossing.

In the first of the papers we place emphasis on scaling properties of flows for which $Ra/Ra_c \leqslant O(10^2)$. The recent work by the Chicago group (Castaing *et al.* 1989) underscores the value of such a treatment. Their main concern was for high-Ra flows and thus our results serves as a contrast to theirs. However, some of the universal features and scalings which we present may also carry over to the high-Ra limit.

2. Formulation and numerical procedures

The Boussinesq approximation to the Navier–Stokes equations in the standard normalization is given by (Chandrasekhar 1961; Drazin & Reid 1981)

$$\frac{\partial \boldsymbol{u}}{\partial t} = -\boldsymbol{u}\cdot\boldsymbol{\nabla}\boldsymbol{u} - \boldsymbol{\nabla}p + Ra\,Pr\,\boldsymbol{e}_z T + Pr\,\nabla^2\boldsymbol{u}, \tag{1a}$$

$$\frac{\partial T}{\partial t} = -(\boldsymbol{u}\cdot\boldsymbol{\nabla})T + w + \nabla^2 T, \tag{1b}$$

where $\boldsymbol{u} = (u, v, w)$ is the velocity, p the pressure, T the departure of the temperature from its (linear) conduction profile, and $\boldsymbol{e}_z$ is a unit vector in the vertical z-direction. All physical quantities have been made dimensionless using the characteristic height of the layer, H, and the thermal diffusivity κ. The dimensionless parameters of the problem are the Rayleigh and Prandtl numbers

$$Ra = \frac{g\alpha\Delta T H^3}{\kappa\nu}, \tag{2a}$$

$$Pr = \frac{\nu}{\kappa}, \tag{2b}$$

where g is the acceleration due to gravity, α is the coefficient of thermal expansion, ΔT the imposed adverse temperature difference and ν the kinematic viscosity.

The case of stress-free boundary conditions

$$w = T = \frac{\partial u}{\partial z} = \frac{\partial v}{\partial z} = 0 \quad \text{on} \quad z = 0, 1 \tag{3}$$

will be considered. Also, the flow will be taken to be L-periodic in the horizontal directions x and y with aspect ratio $L/H = 2\sqrt{2}$, corresponding to the wavelength of maximum linear instability. For this case the critical Rayleigh number is

$$Ra_c = \frac{27\pi^4}{4} = 657.4. \tag{4}$$

In all calculations to be discussed, the Prandtl number is fixed at $Pr = 0.72$. For describing later results it is useful to define the relative Rayleigh number

$$r = Ra/Ra_c. \tag{5}$$

Following procedures described in Tarman (1989) these equations were integrated by means of a pseudospectral code based on that of Herring & Wyngaard (1987). The same code is used here for investigating the flow fields and the reader is referred to

the references for further details. Here we simply note that Fourier collocation is used with de-aliasing based on the 2/3 rule. The time stepping is by a leap-frog scheme for the nonlinear terms and a Crank–Nicholson scheme is used for the diffusion terms. A different version of the code using an Adams–Bashforth scheme for the time stepping yielded nearly indistinguishable results for a $(32)^3$ simulation at $r = 70$. In all runs the time stepping was small enough to satisfy the Courant–Friedrichs–Lewy condition.

3. Eigenfunction analysis

As in Sirovich *et al.* (1989*b*) & Tarman (1989) we use the K-L procedure as a basis for the analysis of chaotic flows. Lumley introduced this method into turbulence theory and it has been widely used since. As originally proposed by Lumley the K-L method was intended as a rational procedure for the extraction of coherent structures. Lumley's work may be regarded as the analytical counterpart of the early work by Theodorsen (1952) and Townsend (1956), which laid the foundation for the concept of coherent structures. In the present investigation we view the K-L procedure as an efficient method for the decomposition and analysis of a chaotic flow. For reasons of continuity and completeness we briefly outline the basic ideas behind this method within the framework of Rayleigh–Bénard convection.

We shall assume that the convective flow is turbulent and the system has been *aged* so that its trajectory lies in the attracting set. Ensemble averages will be denoted by brackets $\langle\,\rangle$. For example, from symmetry it follows that the mean velocity vanishes,

$$\langle \boldsymbol{u} \rangle = 0, \tag{6}$$

and that the mean temperature is independent of x and y,

$$\langle T \rangle = \bar{T}(z). \tag{7}$$

The departure from the mean temperature, $\bar{T}$, will be denoted by the *fluctuation* θ,

$$T = \bar{T} + \theta. \tag{8}$$

It is convenient to define the state vector

$$\boldsymbol{v} = (\boldsymbol{u}, \theta) \tag{9}$$

for the fluctuation having zero mean, $\langle \boldsymbol{v} \rangle = 0$. Since the turbulent flow is time stationary there exists a mean energy

$$E = \langle (\boldsymbol{v}, \boldsymbol{v}) \rangle = \left\langle \int_V \sum_k v_k(\boldsymbol{x}, t)\, v_k(\boldsymbol{x}, t)\, \mathrm{d}\boldsymbol{x} \right\rangle, \tag{10}$$

where V is the volume of the fundamental Rayleigh–Bénard cell, of height H and square planform, $L \times L$. Equation (10) implicitly defines the inner product that will be used in the following.

The K-L procedure now follows by posing the following extremal problem: what is the *most likely instantaneous flow*, say $\phi(\boldsymbol{x})$, in the sense that

$$\lambda = \langle (\phi, \boldsymbol{v})^2 \rangle \tag{11}$$

is a maximum, with ϕ subject to condition (10)? To obtain the answer we form the covariance

$$K_{ij}(\boldsymbol{x}, \boldsymbol{x}') = \langle v_i(\boldsymbol{x}, t)\, v_j(\boldsymbol{x}', t) \rangle \tag{12}$$

and then seek the eigenfunctions, $\phi_k(x)$, such that

$$\int_V \boldsymbol{K}(x, x')\,\phi_k(x')\,\mathrm{d}x' = \lambda_k\,\phi_k(x). \tag{13}$$

The principal eigenfunction of (13) fulfils the requirements of the problem posed above. All subsequent eigenfunctions satisfy the same extremal condition, (11), with appropriate side conditions of orthogonality to the already determined ϕ.

It can be shown (Lumley 1970, 1981; Sirovich 1987*a*) that $\boldsymbol{K}$ is hermitian, non-negative and square integrable (on physical grounds). From this it follows that the *empirical eigenfunctions* $\{\phi_k\}$ form a complete orthonormal set,

$$(\phi_k, \phi_l) = \delta_{kl}. \tag{14}$$

Therefore the base flow, $\boldsymbol{v}$, can be expanded in this set

$$\boldsymbol{v} = \sum a_n\,\phi_n, \tag{15}$$

with

$$a_n = (\phi_n, \boldsymbol{v}). \tag{16}$$

The coefficients $\{a_n\}$ form a statistically orthogonal set,

$$\langle a_n\,a_m\rangle = \lambda_n\,\delta_{nm}. \tag{17}$$

Each eigenvalue, λ_n, can be interpreted as measuring the mean energy of the projected flow energy onto the corresponding eigenspace. In addition it follows that the total mean energy is given by

$$E = \sum_n \lambda_n. \tag{18}$$

As a result of the homogeneity of the problem in the horizontal directions it follows that the empirical eigenfunctions are sinusoidal in x and y (Grenander & Szego 1958; Lumley 1970; Sirovich 1987*b*). We can therefore write a typical eigenfunction as

$$\phi_{kl}^{(n)} = \boldsymbol{\Phi}_{kl}^{(n)}(z)\,\mathrm{e}^{\mathrm{i}2\pi(kx+ly)}, \tag{19}$$

where

$$\int_0^1 \boldsymbol{K}(k, l; z, z')\,\boldsymbol{\Phi}_{kl}^{(n)}(z')\,\mathrm{d}z' = \lambda_{kl}^{(n)}\,\boldsymbol{\Phi}_{kl}^{(n)}(z), \tag{20}$$

and $\boldsymbol{K}(k, l; z, z')$ denotes the Fourier transform of $\boldsymbol{K}$ in the x and y variables. In the following k and l will be referred to as wavenumbers and n as the (vertical) quantum number.

4. Numerical results

A large number of simulations were required because of the aims of this investigation. It is our intention to present a parametric study as the Rayleigh number is varied over a range of values. As we shall see in II, the calculation of Lyapunov dimension requires the determination of a relatively large number of Lyapunov exponents. Each determination of a Lyapunov exponent in turn requires the equivalent of a full simulation. For these reasons we have used a coarser grid than found in the cited studies. In those, a grid of $(32)^3$ points were considered. We also consider 32 points in the vertical but reduce the horizontal grid to $(12)^2$. In the remainder of this section we discuss the basis of this choice and justify it by comparing noteworthy measures of the flow according to the two grid spacings. The use of coarse-grained grids for channel flow has been successfully exploited by Gilbert & Kleiser (1987) and the following deliberations may be relevant to their work.

The most chaotic Rayleigh–Bénard flow that will be considered here is one for which

$$Ra = 70Ra_{\mathrm{c}} \approx 46000. \tag{21}$$

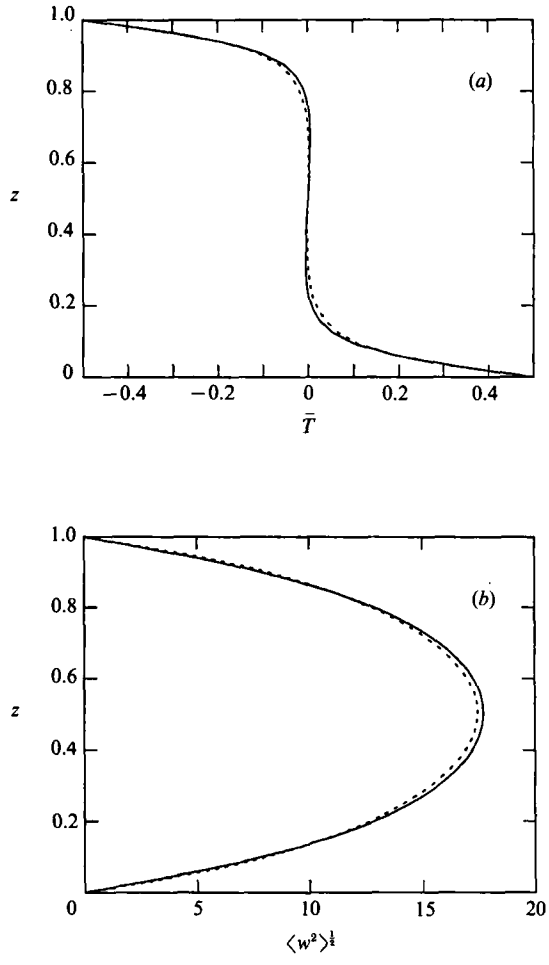

FIGURE 1. (*a*) The mean temperature, $\bar{T}$, and (*b*) the r.m.s. of vertical velocity, $\langle w^2 \rangle^{\frac{1}{2}}$. The solid line indicates the $(32)^3$ calculation and the dashed line the $(12)^2 \times 32$ one.

	$(32)^3$	$32 \times (12)^2$
Nu	5.90	6.12
Re_T	19.5	19.3
S_θ	0.29	0.30

TABLE 1. Nusselt number, Taylor microscale Reynolds number and temperature skewness for the fine-grained and coarse-grained simulations

This is the value used by Herring & Wyngaard in their convection calculation and later by Sirovich *et al.* (1989*b*). In table 1 we compare the Nusselt number, and box-averaged values of the Taylor-microscale Reynolds number, Re_T, and temperature skewness, S_θ (Monin & Yaglom 1975) where

$$S_\theta = -\frac{\langle (\partial u/\partial x)(\partial T/\partial x)^2 \rangle}{\langle (\partial u/\partial x)^2 \rangle^{\frac{1}{2}} \langle (\partial T/\partial x)^2 \rangle} \tag{22}$$

for the coarse- and fine-grain simulations. The agreement is extremely good except

	$(32)^3$			$(12)^2 \times 32$		
	Mode	λ	Deg.	Mode	λ	Deg.
1	(0, 1, 1)	75.137	4	(0, 1, 1)	75.450	4
2	(1, 1, 1)	16.242	4	(1, 1, 1)	16.863	4
3	(0, 1, 2)	7.7384	4	(0, 1, 2)	8.5370	4
4	(0, 0, 1)	6.1013	2	(0, 0, 1)	5.7422	2
5	(0, 2, 1)	5.1559	4	(0, 2, 1)	4.4639	4
6	(1, 2, 1)	3.4338	8	(1, 2, 1)	3.1617	8
7	(0, 1, 3)	3.4146	4	(0, 1, 3)	3.1615	4
8	(1, 1, 2)	2.5981	4	(1, 1, 2)	2.8215	4
9	(0, 2, 2)	2.5263	4	(0, 0, 3)	2.2859	1
10	(0, 3, 1)	2.2208	4	(0, 1, 4)	2.1137	4
11	(1, 1, 3)	2.0764	4	(0, 2, 2)	2.0537	4
12	(0, 1, 4)	1.8146	4	(0, 3, 2)	2.0228	4
13	(0, 0, 3)	1.5815	1	(1, 1, 3)	1.9320	4
14	(0, 2, 3)	1.5491	4	(2, 2, 1)	1.4150	4

TABLE 2. Eigenvalues (λ) of the Karhunen–Loéve modes for the fine-grained and coarse-grained simulations and their degeneracies (deg)

for the Nusselt number, for which there is a 4% error. Note that Nu is higher for the coarse-grained simulation since the truncation of small scales effectively energizes the flow.

The Nusselt number defines a boundary-layer thickness through the relation

$$Nu = \frac{H}{2\delta}. \tag{23}$$

From this and the values of Nu in table 1 we observe that between two and three grid points lie in the boundary layer. Experience has shown that this is more than adequate. The basis for the reduction in horizontal grid points comes from the observation made in Sirovich *et al.* (1989*b*) that wavenumbers such that $k \geqslant 5$ do not occur until the 260th eigenfunction mode. In fact the average energy of the most energetic $k = 5$ mode is less than 0.04% of the total energy. Further justification comes from *a posteriori* comparisons which are now considered.

In figure 1, we present a comparison of the mean temperature $\bar{T}$, and the r.m.s. value of the vertical velocity component, w. As can be seen the agreement is excellent; the percent error based on total variation being 0.17% and 1.9% respectively. A finer assessment of the agreement can be obtained by comparing the empirical eigenfunction decomposition in each instance. We have performed the decomposition using 800 realizations and have used symmetries to extend the data set in the manner described in Sirovich (1987*a*, *b*). Table 2 contains a comparison of the results for the first fourteen *invariant subspaces* in each of the two cases. If we refer back to (20), the first two entries of column two refer to the wavenumber (k, l) and the third to the vertical quantum number, n. The unnormalized eigenvalues appear in column three. The fourth column indicates the degeneracy (corresponding to symmetries of the eigenfunctions) of the subspace. As can be seen the principal eigenvalues agree quite well with each other. Departures become more significant (none worse than about 10%) as we go down the list, but no systematic trend is present. In fact even the ordering is maintained until the ninth invariant subspace, when a mode crossing takes place. Not all of these effects can be attributed to the

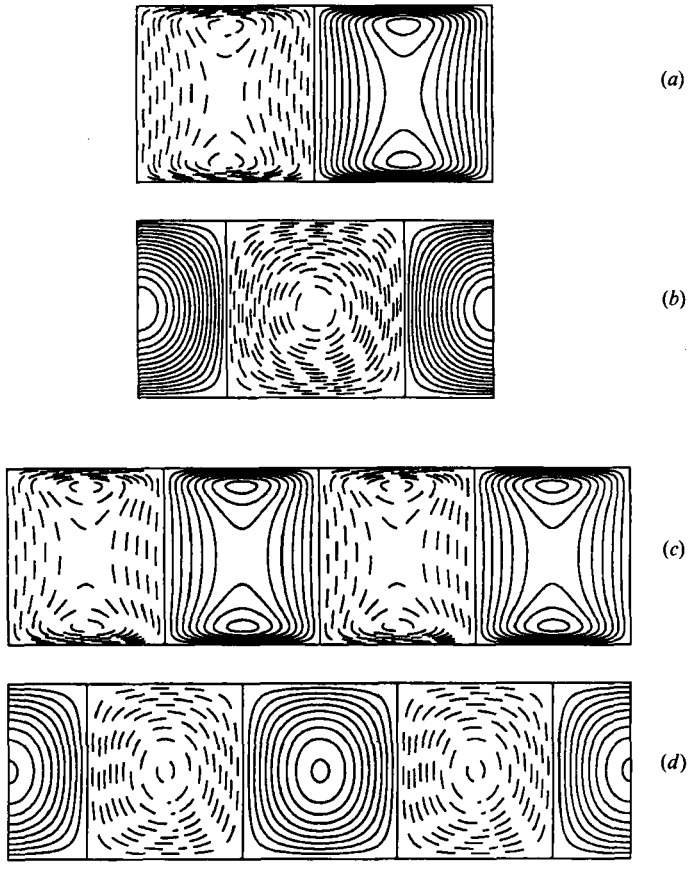

FIGURE 2. (*a*) The isotherms and (*b*) the streamlines corresponding to the principal eigenfunction (0, 1, 1). View is along the x-axis. (*c*) The isotherms and (*d*) the streamlines corresponding to the second eigenfunction (1, 1, 1). View is along the planform diagonal.

difference of grids being used. A similar variation, at fixed grid conditions, is also observed under changes in the length of data records.

Figure 2 contains representative eigenfunctions of the first two invariant subspaces, $\phi_{01}^{(1)}$ and $\phi_{11}^{(1)}$ (see (19)), shown by plotting the corresponding streamlines and isotherms. The first eigenfunction represents a pair of *rolls* aligned along the x- or y-axis while the second is made of four rolls aligned along a diagonal of the square planform. The corresponding fine-grain calculation (Sirovich *et al.* 1989*b*) shows virtually identical structure. The r.m.s. differences between the two sets of calculations are small, being less than 0.5% in the velocity eigenfunctions, and about 2% in the temperature eigenfunction. This robustness in the functional form holds well down into the *stack* of eigenfunctions.

5. Rayleigh-number scaling

In as much as the coarse-grained calculation at $r = 70$ is adequately resolved, we are also able to consider $r < 70$, in which case the resolution improves with decreasing r. We have made a detailed investigation at five moderate values of Rayleigh number for which we find chaotic behaviour:

$$r = 5, 15, 30, 50, 70, \tag{24}$$

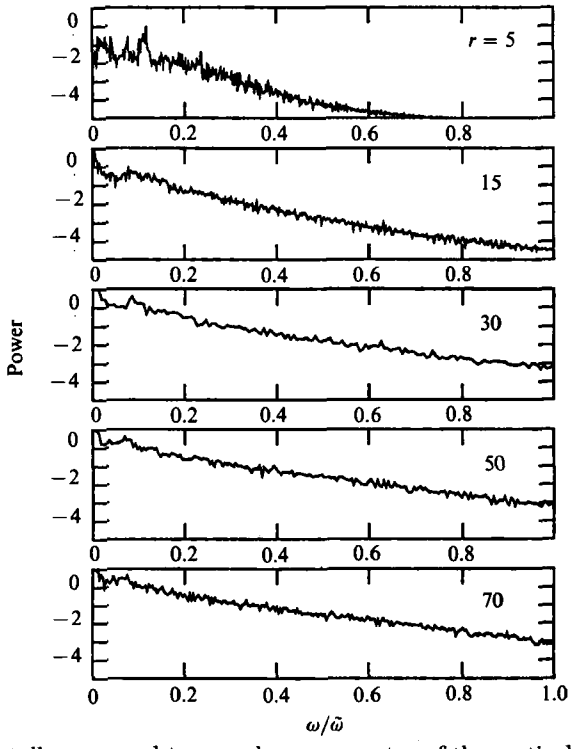

FIGURE 3. Horizontally averaged temporal power spectra of the vertical velocity in the midplane $z = \frac{1}{2}$ at the indicated value of Rayleigh number. The frequency has been scaled according to $r^{-\frac{2}{3}} \times 10^{-2}$.

where the lower value is chosen by the appearance of irregular behaviour and the upper value by the adequacy of resolution. In figure 3 we show the power spectra of the vertical velocity, w, recorded at the midplane for $r = 5$–70. The spectra have been averaged over sixteen points in the mid-plane. At $r = 5$ we have what might be termed noisy periodicity (Lorenz 1980), while at $r = 70$ the spectrum has the broadband features associated with chaos. At the intermediate values of r the spectra appear similar to that for $r = 70$. The transition in character, as the Rayleigh number is increased, can also be observed in the change in autocorrelation. This is discussed in II. Here we simply note that, as Ra increases, the periodic component rapidly decreases in strength, but is still present at $r = 70$, leading to a decaying but oscillatory autocorrelation over the entire range of r.

In plotting the five power spectra of figure 3, the frequency has been normalized with repect to

$$\tilde{\omega} \propto r^{\frac{2}{3}}; \tag{25}$$

we show in II that this is the appropriate frequency scaling. As is clear from figure 3 the power spectrum appears to take on a universal form in the shape of an exponential at the higher values of Ra. The spectra at $r = 50$ and $r = 70$ virtually lie on one another.

5.1. *Probability distribution functions*

The Chicago group (Castaing *et al.* 1989) have shown that one of the distinguishing features of *soft* and *hard* turbulence is the respective presence of either a Gaussian or an exponential distribution for temperature fluctuations. It is of interest to see the

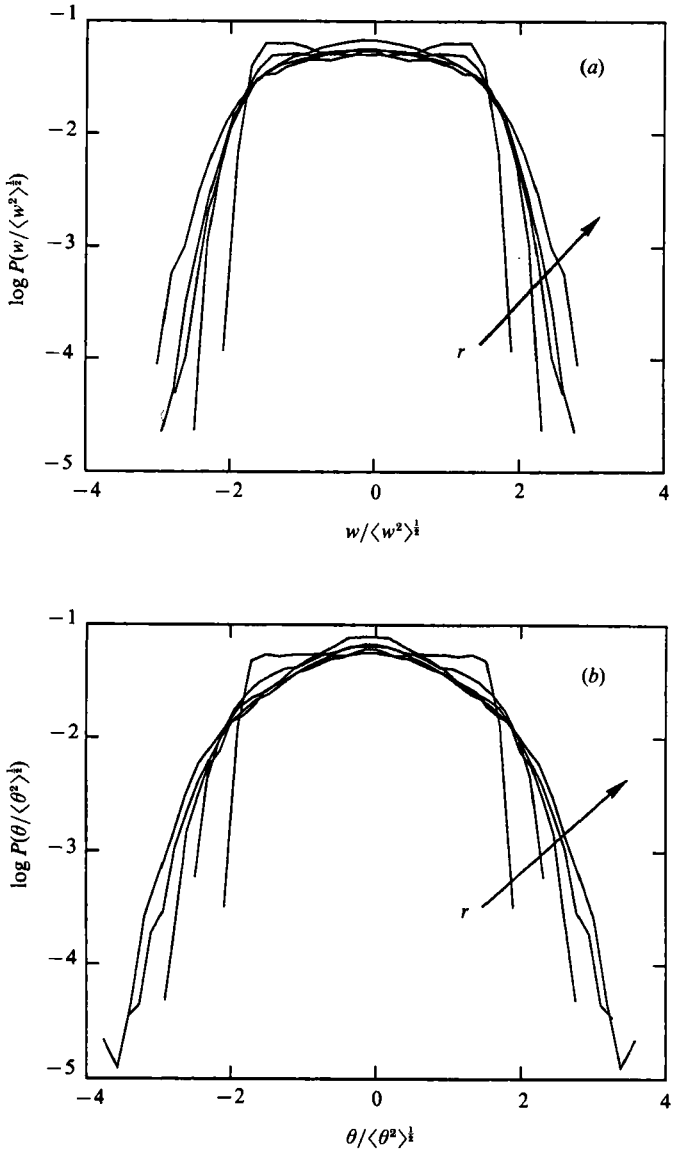

FIGURE 4. The probability density functions of (*a*) the vertical velocity w and (*b*) the temperature, both in the midplane for different Rayleigh numbers. Each p.d.f. has unit variance. The direction of the arrow indicates increasing values of r.

passage to the normal distribution as Ra increases in the limited range being considered here. This is shown in figure 4. Figure 4(*a*) shows the distribution of vertical velocity fluctuations and figure 4(*b*) the distribution of temperature fluctuations. Both of these distributions have been calculated at the midplane. (Each p.d.f. has been normalized so that there is unitary variance.) Both the temperature and velocity p.d.f.s are seen to be Gaussian at the higher values of r. At the lower values of r the p.d.f.s are quite flat and in fact the velocity p.d.f. is seen to be bimodal at $r = 5$. The flat p.d.f.s at lower values of r appear because the motion is dominated by large rolling modes. This will be discussed further later.

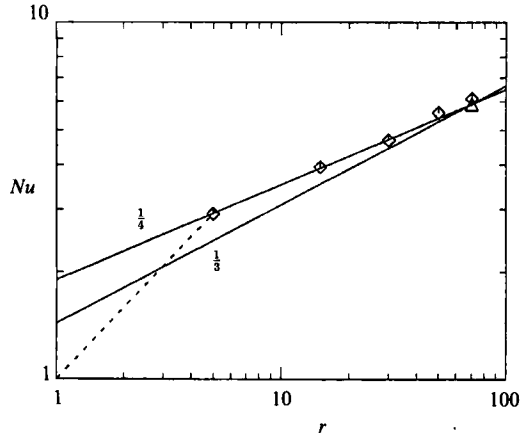

FIGURE 5. Nusselt number versus Rayleigh number. The solid lines have slopes 1/4 and 1/3 and the dashed line indicates that the Nusselt number is unity at $r = 1$. The diamonds are at calculated values of Nu with $(12)^2 \times 32$ resolution while the triangle is with $(32)^3$ resolution. Note that for $r = 70$ there is discernable error in Nu.

	$r = 5$	15	30	50	70
Nu	2.91	3.94	4.69	5.59	6.12
Re_T	8.5098	12.620	14.487	18.407	19.329
S_θ	0.198	0.226	0.254	0.289	0.297

TABLE 3. Nusselt number, Taylor microscale Reynolds number and temperature skewness for simulations at the indicated Rayleigh numbers

5.2. *Nusselt number*

Table 3 contains the results at the five values of r for the Nusselt number, Reynolds number and skewness. The weakly turbulent nature of the flow is apparent from the low values of Re_T and the skewness. The Re_T data have a power-law behaviour of the form $Re_T \sim r^{0.28}$.

Figure 5 contains a plot of the Nusselt number as function of Rayleigh number. A data point from the fine-grained calculation, at $r = 70$, is indicated as a triangle. The coarse-grained data at smaller values of r, together with the fine-grained data point appear to be well fitted by a straight line of slope 0.25, i.e.

$$Nu \propto \left(\frac{Ra}{Ra_c}\right)^{\frac{1}{4}} \tag{26}$$

for the range given in (24). Although the difference between the fine- and coarse-grained calculations is small, roughly 4% at $r = 70$, the difference is discernible in figure 5. The overestimate in Nu by the coarse-grain treatment is understandable since diminished resolution results in diminished dissipation. Hence the flow is *overenergetic*, which results in greater heat transport due to convection.

Equation (26) should be contrasted with the often mentioned value of

$$Nu \propto \left(\frac{Ra}{Ra_c}\right)^{\frac{1}{3}}, \tag{27}$$

which is also shown in the figure. The quarter-power law, (26), has been obtained theoretically by Pillow (1952). Pillow's argument is basically a two-dimensional one which rests on heat transfer computed by cellular convection modes based on the eigenfunctions of linear theory. It leads to an increasing exponent in (26) or (27) (Malkus 1954*a*, *b*; Catton 1966) and hence more efficient heat transfer as Ra increases, so more modes need to be included. The same argument applies here. Now however the modes are the empirical eigenfunctions which are more truly representative of the nonlinear flow. As we indicate later the overwhelming amount of energy of motion in all of the simulations is a two-dimensional cellular motion – but one that orients itself along the x- and y-axes at random times. The argument is still valid since we have computed the switching time of the eddy and it is at least an order of magnitude larger than the eddy turnover time. The dominant mode is the $(0, 1, 1)$ mode and may be thought of as the *wind* in the problem in the same spirit as the Chicago group experiment (however, there is no indication of plume structures being generated for the limited range of Ra investigated here). There is therefore a sound basis for applying Pillow's argument to the present case and hence for the quarter-power law, (26), to be applicable here. The fact that Pillow considers no-slip boundary conditions and ours are slip boundaries should be of little consequence since the primary mechanism for the heat transport in this picture is the cellular motion in the main body of the flow.

Another theoretical treatment leading to a power law is due to Catton (1966) who obtained

$$Nu \propto \left(\frac{Ra}{Ra_c}\right)^{0.29}. \tag{28}$$

His treatment is based on a count of the linear modes which become unstable as the Rayleigh number is incremented. This treatment was based on the earlier suggestion by Malkus. Laboratory confirmation of such power laws have also been obtained. Garon & Goldstein (1973) report an exponent of 0.29 and Threlfall (1975) found an exponent of 0.28. More recently, the Chicago group have found the one-third exponent, in a soft turbulence regime, and an exponent of $\frac{2}{7}$ in the hard turbulence regime, the regimes being distinguished by the nature of probability distributions.

There are wide differences in conditions amongst the various studies we have been discussing and just a few points will be mentioned. Unlike the cited references, our boundary condition are of slip type, but as mentioned above this is not felt to be important if we consider Nu versus r. Our simulations cover a relatively narrow band of Rayleigh numbers in what must be regarded as the low-turbulence range. In fact as a result of the relatively low value of r, significant cross-talk between the flow at the two bounding planes should be expected. However, the standard argument for obtaining the $\frac{1}{3}$ slope is based on the premise that the plate separation should become unbounded (Turner 1973) and hence that the cross-talk diminish as Ra increases.

5.3. *Scalings*

In our parametric study we find that temperatures and velocities scale quite well with the scalings introduced in Sirovich *et al.* (1989*b*). A characteristic velocity in the boundary layer is

$$u_c = (2g\alpha\Delta T\delta)^{\frac{1}{2}}, \tag{29}$$

which in the standard normalization with respect to the thermal diffusion is

$$\hat{u}_c = \frac{u_c}{\kappa/H} = \left(\frac{Ra\,Pr}{Nu}\right)^{\frac{1}{2}}. \tag{30}$$

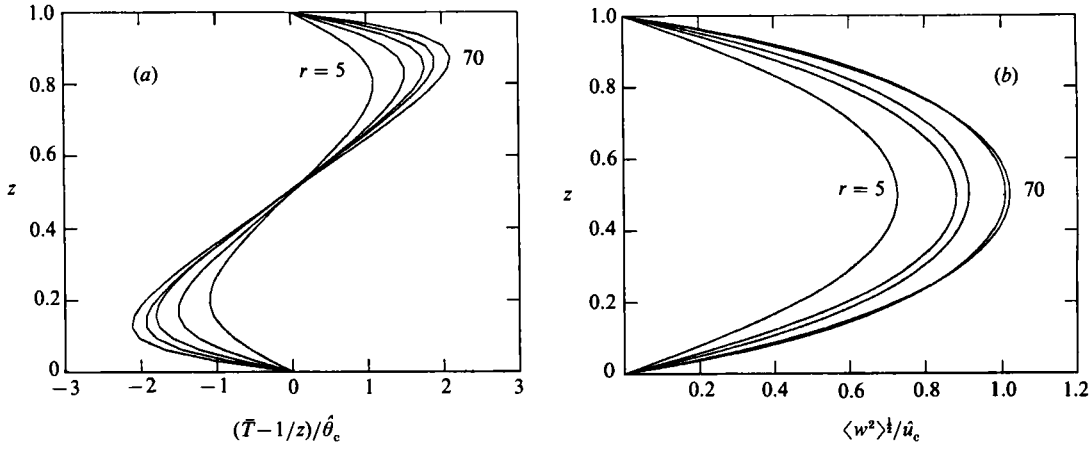

FIGURE 6. (*a*) The mean temperature $\bar{T}$ and (*b*) the r.m.s. of the vertical velocity at various values of r.

A characteristic temperature is obtained by demanding that the turbulent heat flux in the centre of the cell be equal to that due to diffusion at the boundary:

$$u_c \theta_c = \kappa \frac{\Delta T}{2\delta}, \tag{31}$$

which leads to

$$\hat{\theta}_c = \frac{\theta_c}{\Delta T} = \left(\frac{Nu^3}{Ra\,Pr}\right)^{\frac{1}{2}}. \tag{32}$$

It is of interest to observe the change in the mean temperature profile $\bar{T}$ and $\langle w^2\rangle^{\frac{1}{2}}$ as the Rayleigh number is varied, particularly with regard to the scalings. This is shown in figure 6 where they have been scaled according to (30) and (32). At the higher values of the Rayleigh number the scalings appear to hold very well, being nearly indistinguishable in the case of the velocity profile. Note that the boundary-layer thickness scales as in (23), a fact that will be used in the spectral scalings presented below.

6. Flow decomposition

We now consider the flow in detail by performing the K-L expansion on the simulations at the five Rayleigh numbers, (24). Except for the case $r = 70$ already discussed, we use 300 realizations and use symmetries in all cases to expand the data sets. The results are summarized in table 4, which shows the modes, their percent energy contribution to the total, and their degeneracy based on their symmetry. Several features are worth noting. As the Rayleigh number is decreased the first few modes capture an increasingly large share of the energy. In fact at $r = 5$ the first mode itself captures 65% of the energy. In a probabilistic sense, the flow spends 65% of its time executing this motion. The dominance of this at $r = 5$ also shows in the p.d.f. discussed earlier and shown in figure 4, where it is seen that the distribution is bimodal. At this low value of r the rolling motion penetrates through the middle of the layer where the p.d.f. is measured. This results in an emphasis of the non-zero vertical motion. At higher values of r the smaller scales become more important and thus flatten the p.d.f.

	$r = 5$			15			30			50			70		
	Mode	Energy	Deg.	Mode	Energy	Deg.	Mode	Energy	Deg.	Mode	Energy	Deg.	Mode	Energy	Deg.
1	(0, 1, 1)	64.9	4	(0, 1, 1)	51.8	4	(0, 1, 1)	43.2	4	(0, 1, 1)	42.4	4	(0, 1, 1)	39.2	4
2	(1, 1, 1)	19.3	4	(1, 1, 1)	14.3	4	(1, 1, 1)	12.6	4	(1, 1, 1)	11.8	4	(1, 1, 1)	8.76	4
3	(0, 1, 2)	4.40	4	(0, 1, 2)	4.93	4	(0, 1, 2)	5.72	4	(0, 1, 2)	5.61	4	(0, 1, 2)	4.44	4
4	(1, 2, 1)	2.61	8	(0, 0, 1)	1.06	2	(0, 0, 1)	1.23	2	(0, 0, 1)	1.27	2	(0, 0, 1)	1.49	2
5	(0, 2, 1)	1.05	4	(1, 2, 1)	3.95	8	(1, 2, 1)	3.91	8	(1, 2, 1)	3.57	8	(0, 2, 1)	2.32	4
6	(0, 1, 3)	0.092	4	(0, 2, 1)	1.94	4	(0, 2, 1)	1.87	4	(0, 2, 1)	1.63	4	(1, 2, 1)	3.29	8
7	(0, 0, 1)	0.021	1	(0, 0, 3)	0.45	1	(0, 2, 2)	1.77	4	(1, 1, 2)	1.54	4	(0, 1, 3)	1.64	4
8	(1, 1, 2)	0.054	4	(0, 1, 3)	1.56	4	(0, 1, 3)	1.37	4	(0, 1, 3)	1.13	4	(1, 1, 2)	1.47	4
9	(1, 1, 3)	0.049	4	(0, 1, 4)	1.26	4	(0, 1, 4)	1.30	4	(0, 1, 4)	1.09	4	(0, 0, 3)	0.30	1
10	(0, 3, 1)	0.046	4	(0, 2, 2)	1.23	4	(1, 1, 2)	1.24	4	(0, 2, 2)	1.04	4	(0, 1, 4)	1.10	4

TABLE 4. Eigenvalues of the Karhunen–Loéve modes as a function of (k_1, k_2, q) for the indicated values of the Rayleigh number. The modes $k_1 = k_2 = 0$ can be either purely mechanical (degeneracy two) or purely thermal (degeneracy one).

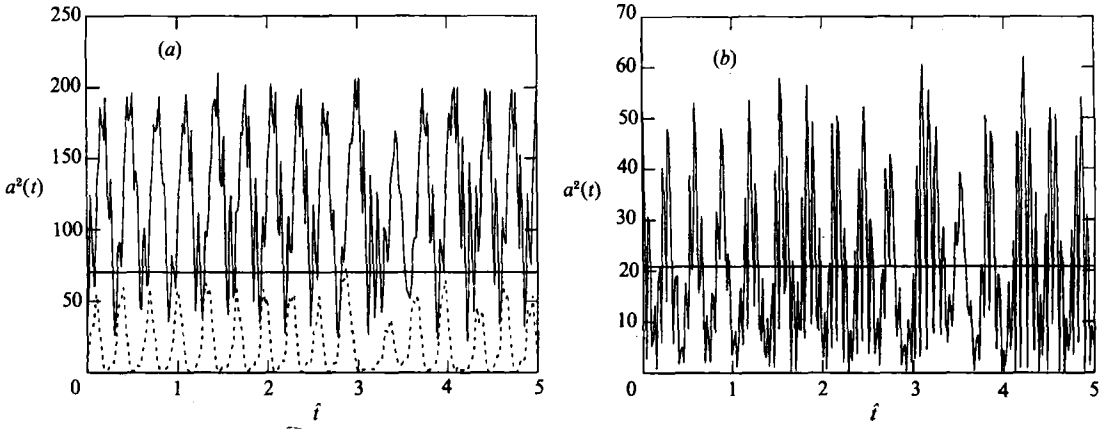

FIGURE 7. Typical evolution of energy at $r = 5$ (see (16)) of the empirical eigenfunctions. (*a*) The modes (0, 1, 1) (solid line) and (1, 0, 1) (dashed line). (*b*) The modes (1, 1, 1) (solid line) and (−1, 1, 1) (dashed line). The horizontal line in both figures represents the average energy or eigenvalue of the mode including degeneracies. Time has been rescaled according to $\hat{t} = t/r^{\frac{1}{2}}$, see (25).

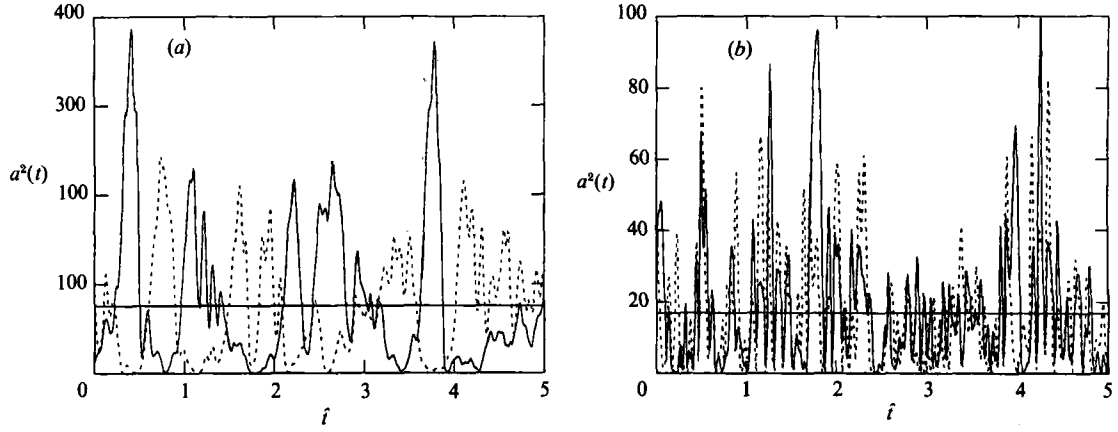

FIGURE 8. As in figure 7 but for $r = 70$.

At the higher end of the table, $r = 70$, 39% of the energy resides in this first mode. Balachandar, Maxey & Sirovich (1989) and Sirovich, Balachandar & Maxey (1989*a*) have shown that at $r = 9800$ this first mode still contains 25% of the energy. It is therefore of interest to think about the asymptotic limit, $Ra \uparrow \infty$. From the limited data it appears that the energy in this first mode falls to zero with some inverse power, $\lambda_{01}^1 \propto r^{-\nu}$. (From the fragmentary information, $\nu \approx 0.1$.) We also note from table 4 that while the first three most energetic modes are (0, 1, 1), (1, 1, 1) and (0, 1, 2) over the range of Ra, there are a number of mode crossings that take place down the stack of eigenfunctions – different modes become active as Ra is varied. This is particularly true at the lower values of r.

The spatial structure of a given eigenfunction consists of a horizontal and a vertical part. The horizontal part is sinusoidal, (19), and thus does not vary with Ra. The vertical part in general simplifies with decreasing Ra in that fewer harmonics participate as Ra is decreased. Tarman (1989) describes the spatial structure of a large number of modes at $r = 70$. The spatial structure of two of the most energetic

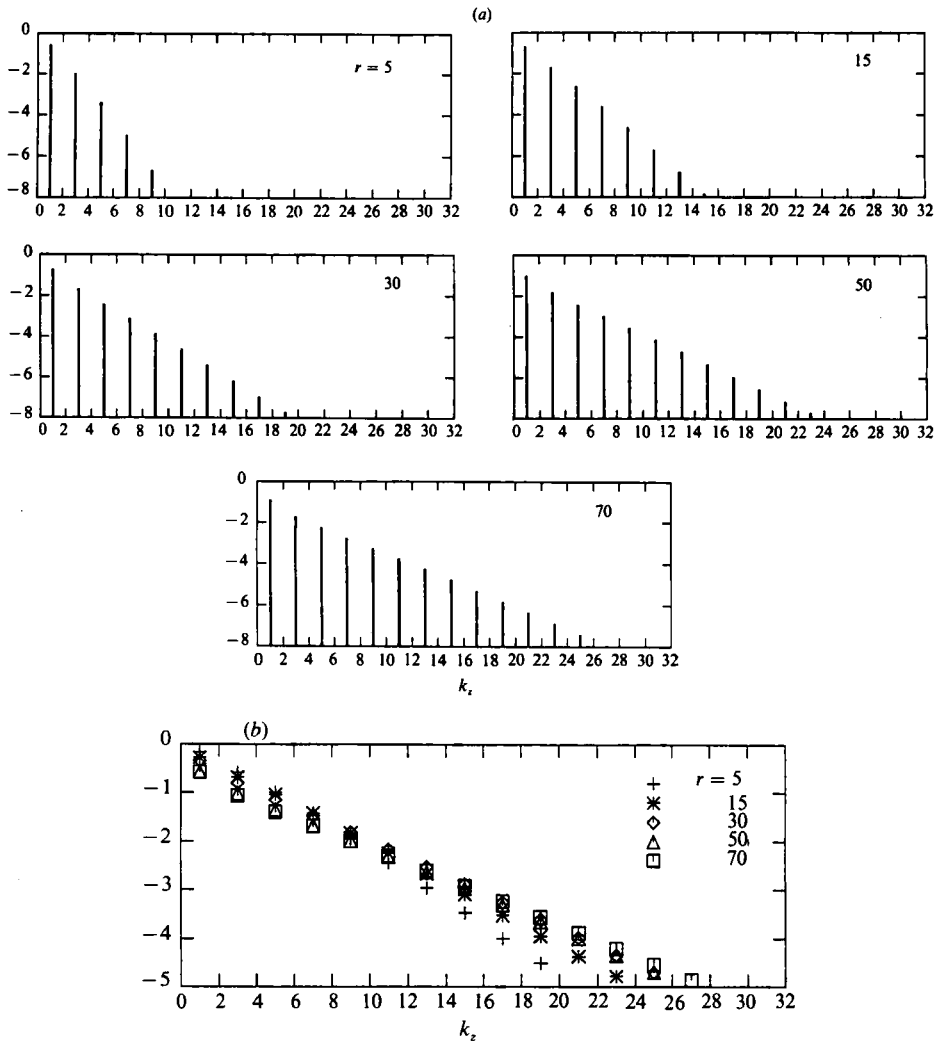

FIGURE 9. (*a*) The harmonic content of the temperature eigenfunction (0, 1, 1) for various values of r. (*b*) The scaling of eigenfunctions with Nusselt number. Shown in the power in the (0, 1, 1) scaled with the Nusselt number as exponent $-\log(P)^{Nu/10}$.

modes was discussed earlier in §4 (figure 2). The motion is in the form of rolls and the temperature fluctuations take on a double-lobed appearance on either side of a convective roll. Other modes have different character. The (0, 0, 1) mode, for example, (table 4) is purely mechanical – no temperature fluctuations occur and the motion is confined to $z = \text{const}$. The mode (0, 0, 3), on the other hand, is purely thermal with no associated motion. In general, as the vertical quantum number is increased, the number of zero-crossings increase (as seen for example in Sturm–Liouville eigenfunctions).

Once the eigenfunctions have been calculated the flow can be projected onto this space and the evolution of the energy in each mode determined. This is shown for the first two eigenfunctions in figures 7 and 8 for $r = 5$, and 70 respectively. Turning our attention to the principal mode (0, 1, 1) (figures 7*a* and 8*a*) we observe that at $r = 5$

most of the energy is maintained in a two-roll cell aligned along the y-axis, the corresponding roll along the x-axis gaining little energy for this relatively short duration. At $r = 70$ (and at $r > 5$, not shown) on the other hand, the motion is faster and the rolls alternate in energy. In the mode (1, 1, 1) (figures 7*b* and 8*b*) which corresponds to four rolls aligned along one diagonal of the square planform, at $r = 5$ the rolls along the other diagonal evolve virtually identically. At $r = 70$ (and at $r > 5$ not shown) there are discernable amplitude variations but the two sets of rolls mostly maintain phase. Thus the nature of the flow at $r = 5$, consisting of rolls which remain aligned with one axis for long periods of time, appears characteristically different from that at $r > 5$, where rolls randomly align themselves with the x- and y-axis. The observed chaos at $r = 5$, which is low-dimensional (see II), is therefore mostly associated with the temporal evolution of the first and second modes and not with the spatial structure, which remains fairly well organized. In addition note that time has been rescaled in figures 7 and 8; the oscillations are also more rapid at large r in unscaled coordinates. The oscillations at a given r are more rapid for the higher modes (modes with lesser energy).

We close this section by discussing the variations in the eigenfunctions with Ra. In figure 9(*a*) we plot the spatial power spectrum in the z-direction of the temperature portion of the (0, 1, 1)-mode at the five values of r. As expected the harmonic content in the vertical direction decreases with decreasing r, and tends to an almost pure sinusoid at $r = 5$. In view of the fact that the thermal layer scales with the inverse Nusselt number, it would seem reasonable that we plot the spatial power versus k/Nu. If we make use of the near exponential behaviour of the spectrum we obtain figure 9(*b*). From this it appears that the spectrum is tending to a *universal* form. In view of the limited range of our data base this indication requires further verification.

7. Discussion

As the Rayleigh number is decreased, we anticipate that the motion should become more sluggish, and that fewer modes should be implicated in the motion. The latter is confirmed in table 4, where we have seen that an increasing fraction of energy is contained in the first few modes as r is decreased. The question of dimension will be discussed in some detail in II. For the moment, however, it goes almost without saying that the dimension of the system diminishes as the Rayleigh number decreases.

In view of the many treatments of the Bénard problem by highly truncated modal models (Malkus & Veronis 1958; Toomre, Gough & Spiegel 1977, 1982; Massaguer & Mercader 1988; F. H. Busse 1989 private communication) it is of interest to compare the K-L eigenfunctions with those used in the modal treatments. It is therefore implicit to the following discussion that the eigenfunctions or modes are to be used to derive a dynamical system or to be used in the way that Malkus (1954*a*, *b*) envisioned in his pioneering papers, using the eigenfunctions of linear stability theory. (See also Spiegel 1962 who further suggests using the *mean field* eigenfunctions.) Thus, for the case of slip boundary conditions each is given by a product of three sinusoids. In other words, these eigenfunctions are *monochromatic* in each of three directions. As figure 9(*a*) shows, the empirical eigenfunctions approach the modal eigenfunctions as Ra is decreased. At even modest values of Ra, however, the empirical eigenfunctions are richer and better able to capture the steepening nonlinear profiles. Figure 10, which shows the temperature eigenfunctions in the spatial domain, indicates how, as the Rayleigh number is increased, the presence of

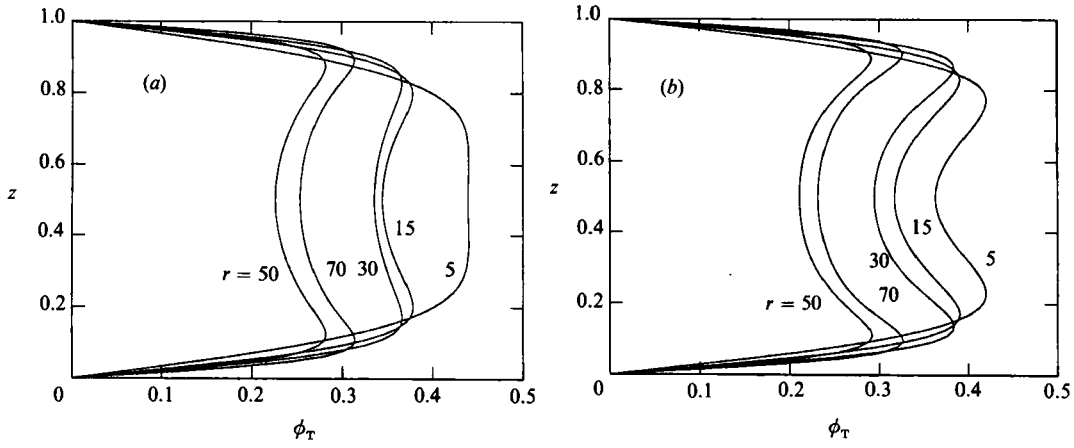

FIGURE 10. The temperature eigenfunctions in the spatial domain for various values of r.

additional harmonics changes this profile into the double-lobed structure visible for instance in figures 2(*a*) and 2(*c*). There is one important additional simplifying feature of the empirical eigenfunctions which bears mention. In the modal approach one scalar function of time appears for each harmonic combination, and for each dependent variable. On the other hand in our procedure the eigenmodes are organized so that only one function of time appears for all four components $(\boldsymbol{u}, \theta)$. Therefore only a third of the number of dependent variables has to be considered.

To conclude: In this paper we have studied convection under highly idealized conditions. A detailed analysis of the weakly turbulent flow found at relatively low Ra has been performed. Gross features (Nu, Re_T, etc) are found to possess scalings, although it is known that the particular coefficients and exponents are not valid at large Ra. The K-L decomposition has been used to elucidate the physics of these complex flows in a quantitative manner. An examination of the structure of the empirical eigenfunctions has revealed important apparent scaling with Ra. Should these scalings hold for asymptotically large Ra in Rayleigh–Bénard convection with different boundary conditions and geometries they would provide structural details of the flow field without explicit simulation.

The work reported here was supported by DARPA-URI N00014-86-K0754. The authors gratefully acknowledge the use of the Pittsburgh Supercomputing Center at which our calculations were carried out.

REFERENCES

ASH, R. B. & GARDNER, M. F. 1975 *Topics in Stochastic Processes*. Academic.

AUBRY, N., HOLMES, P., LUMLEY, J. L. & STONE, E. 1988 The dynamics of coherent structures in the wall region of a turbulent boundary layer. *J. Fluid Mech.* **192**, 115.

BALACHANDAR, S., MAXEY, M. R. & SIROVICH, L. 1989 Numerical simulation of high Rayleigh number convection. *J. Sci. Comput.* **4**, 219.

BENETTIN, G., GALGANI, L., GIORGILLI, A. & STRELCYN, J.-M. 1980 Lyapunov characteristic exponents for smooth dynamical systems and Hamiltonian systems: A method for computing all of them. Pts. 1 and 2. *Meccanica* **15**, 9–30.

BUSSE, F. H. 1985 In *Hydrodynamic Instabilities and the Transition to Turbulence* (ed. H. L. Swinney & J. P. Gollub). Springer.

CASTAING, B., GUNARATNE, G., HESLOT, F., KADANOFF, L., LIBSCHABER, A., THOMAE, S., WU, X-Z., ZALESKI, S. & ZANETTI, G. 1989 Scaling of hard thermal turbulence in Rayleigh–Bénard convection. *J. Fluid Mech.* **204**, 1.

CATTON, I. 1966 Natural convection in horizontal liquid layers. *Phys. Fluids* **19**, 252.

CHANDRASEKHAR, S. 1961 *Hydrodynamic and Hydromagnetic Stability*. Oxford University Press.

CONSTANTIN, P., FOIAŞ, C., MANLEY, O. P. & TEMAM, R. 1985 Determining modes and fractal dimension of turbulent flows. *J. Fluid Mech.* **150**, 427.

DRAZIN, P. G. & REID, W. H. 1981 *Hydrodynamic Stability*. Cambridge University Press.

FEIGENBAUM, M. J. 1978 Quantitative universality for a class of nonlinear transformations. *J. Statist. Phys.* **19**, 25.

FENSTERMACHER, P. R., SWINNEY, H. L. & GOLLUB, J. P. 1979 Dynamical instabilities and the transition to chaotic Taylor vortex flow. *J. Fluid Mech.* **94**, 103.

FOIAŞ, C., MANLEY, O. & TEMAM, R. 1987 *Nonlin. Anal. Theory, Meth. Applics.* **11**, 939–967.

GARON, A. M. & GOLDSTEIN, R. J. 1973 Velocity and heat transfer measurements in thermal convection. *Phys. Fluids* **16**, 1818–1825.

GILBERT, N. & KLEISER, L. 1987 Low-resolution simulations of transitional and turbulent channel flow. In *Proc. Intl Conf. on Fluid Mechanics*. Peking University Press, Beijing, China.

GLAUSER, M. N., LIEB, S. J. & GEORGE, N. K. 1987 Coherent structure in the axisymmetric jet mixing layer. In *Turbulent Shear Flows 5* (ed. F. Durst *et al.*). Springer.

GRENANDER, U. & SZEGO, G. 1958 *Toeplitz Forms and Their Application*. University of California Press, Berkeley.

HERRING, J. H. & WYNGAARD, J. 1987 Convection with a simple chemically reactive passive scalar. 10.39–10.43 In *Turbulent Shear Flows 5* (ed. F. Dust *et al.*), p. 328. Springer.

KAPLAN, J. & YORKE, J. 1979 Chaotic behavior in multi-dimensional difference equations. In *Functional Differential Equations and the Approximation of Fixed Points* (ed. H. O. Peitgen & H. O. Walther). In Lecture Notes in Mathematics, vol. 730, p. 228. Springer.

KEEFE, L. & MOIN, P. 1987 *Bull. Am. Phys. Soc.* II **32**, 2026.

LANDAU, L. D. 1944 *Dokl. Akad. Nauk. SSSR* **44**, 339.

LORENZ, E. N. 1959 Prospects for statistical weather forecasting. *Final Rep., Statistical Forecasting Project, MIT.*

LORENZ, E. N. 1963 Deterministic nonperiodic flow. *J. Atmos. Sci.* **20**, 130.

LORENZ, E. N. 1980 Noisy periodicity and reverse bifurcation. In *Nonlinear Dynamics* (ed. R. H. G. Helleman). NY Acad. Sci.

LUMLEY, J. L. 1967 The structure of inhomogeneous turbulent flows. In *Atmospheric Turbulence and Radio Wave Propagation* (ed. A. M. Yaglom & V. I. Tatarski), pp. 166–178. Moskow: Nauka.

LUMLEY, J. L. 1970 *Stochastic Tools in Turbulence*. Academic.

LUMLEY, J. L. 1981 Coherent structures in turbulence. In *Transition and Turbulence* (ed. R. E. Meyer), pp. 215–242. Academic.

MALKUS, W. V. R. 1954*a* Discrete transitions in turbulent convection. *Proc. R. Soc. Lond.* **225**, 185.

MALKUS, W. V. R. 1954*b* The heat transport and spectrum of thermal turbulence. *Proc. R. Soc. Lond.* **225**, 198.

MALKUS, W. V. R. & VERONIS, G. 1958 Finite amplitude cellular convection. *J. Fluid Mech.* **4**, 225.

MALRAISON, D., ATTEN, P., BERGÉ, P. & DUBOIS, M. 1983 Dimension d'attracteurs étranges: une détermination expérimentale en régime chaotique de deux systéms convectifs. *CR Acad. Sci. Paris* **C297**, 209.

MASSAGUER, J. M. & MERCADER, I. 1988 Instability of swirl in low-Prandtl-number thermal convection. *J. Fluid Mech.* **189**, 367.

MOIN, P. 1984 Probing turbulence via large eddy simulation. *AIAA Paper*-84-0174.

MOIN, P. & MOSER, R. D. 1989 Characteristic-eddy decomposition of turbulence in a channel. *J. Fluid Mech.* **200**, 471.

MONIN, A. S. & YAGLOM, A. M. 1975 *Statistical Fluid Mechanics* Vol. II. MIT Press.

PILLOW, A. F. 1952 The free convection cell in two dimensions. *Rep. Aero. Res. Lab. Melbourne* A79.

PREISENDORFER, R. W. 1988 Principal component analysis in meteorology and oceanography. In *Meteorology and Oceanography*. Elsevier.

RUELLE, D. & TAKENS, F. 1971 On the nature of turbulence. *Commun. Math. Phys.* **20**, 167.

SHIMADA, I. & NAGASHIMA, T. 1979 A numerical approach to the ergodic problem of dissipative dynamical systems. *Prog. Theor. Phys.* **61**, 1605.

SIROVICH, L. 1987*a* Turbulence and the dynamics of coherent structures, Pt. I: Coherent Structures. *Q. Appl. Maths* **XLV**, 561.

SIROVICH, L. 1987*b* Turbulence and the dynamics of coherent structures, Pt. II. Symmetries and transformations. *Q. Appl. Maths* **XLV**, 573.

SIROVICH, L., BALACHANDAR, S. & MAXEY, M. R. 1989*a* Simulations of turbulent thermal convection. *Phys. Fluids* A **1**, 1911–1914.

SIROVICH, L. & DEANE, A. E. 1991 A computational study of Rayleigh–Bénard convection. Part 2. Dimension considerations. *J. Fluid Mech.* **222**, 251 (referred to herein as II).

SIROVICH, L., MAXEY, M. & TARMAN, H. 1989*b* Analysis of turbulent thermal convection. In *Sixth Symposium on Turbulent Shear Flow, Toulouse, France*, p. 68. Springer.

SIROVICH, L. & RODRIGUEZ, J. D. 1987 Coherent structures and chaos: A model problem. *Phys. Lett* A **120**, 211–214.

SPIEGEL, E. A. 1962 *On the Malkus Theory of Turbulence*, p. 181. Centre National de la Researche Scientifique, Paris.

TARMAN, H. 1989 Analysis of turbulent thermal convection. Ph.D. thesis, Brown University.

TARMAN, H. & SIROVICH, L. 1990 Low dimensional dynamics for the turbulent convection problem (to appear).

THEODORSEN, T. 1952 Mechanism of turbulence. In *Proc. 2nd Midwestern Conf. on Fluid Mech., Ohio State Univ., Columbus, Ohio.*

THRELFALL, D. C. 1975 Free convection in low-temperature gaseous helium. *J. Fluid Mech.* **67**, 17.

TOOMRE, J., GOUGH, D. O. & SPIEGEL, E. A. 1977 Numerical solutions of single-mode convection equations. *J. Fluid Mech.* **79**, 1.

TOOMRE, J., GOUGH, D. O. & SPIEGEL, E. A. 1982 Time-dependent solutions of multimode convection equations. *J. Fluid Mech.* **125**, 99.

TOWNSEND, A. A. 1956 *The Structure of Turbulent Shear flow*. Cambridge University Press.

TURNER, J. S. 1973 *Buoyancy Effects in Fluids*. Cambridge University Press.

WOLF, A., SWIFT, J. B., SWINNEY, H. L. & VASTANO, J. A. 1985 Determining Lyapunov exponents from a time series. *Physica* **16D**, 285.